DOI:10.13476/j.cnki.nsbdqk.2020.0048
段浩,赵红莉,蒋云钟. 遥感 Penman-Monteith 模型中土壤含水量与土壤蒸发的关系[J]. 南水北调与水利科技(中英文),2020,18(3):31-47. DUAN H,ZHAO H L,JIANG Y Z. Assessment the relationship between soil evaporation and soil moisture using remote sensing Penman-Monteith model[J]. South-to-North Water Transfers and Water Science & Technology,2020,18(3):31-47. (in Chinese)

遥感 Penman-Monteith 模型中土壤含水量与土壤蒸发的关系

段浩,赵红莉,蒋云钟

(中国水利水电科学研究院 水资源研究所,北京 100038)

摘要:土壤含水量是影响土壤蒸发的重要因素,分析土壤含水量变化对土壤蒸发的影响,对水资源管理有积极作用。遥感 Penman-Monteith(P-M)模型是利用遥感手段进行蒸散发模拟的重要方法,且能分别对土壤蒸发和植被散发进行计算。利用遥感 P-M 模型对望都站的蒸散发进行模拟,并结合地表土壤含水量数据分析了土壤含水量变化对模型参数及土壤蒸发的影响。结果表明:遥感 P-M 模型对望都站蒸散发取得较好效果,纳什效率系数(NSE)为 0.559;土壤含水量变化与遥感 P-M 模型的土壤蒸发系数间具有不确定性;在本研究的模拟期内,与植被散发相比,土壤含水量变化与土壤蒸发间的一致性更强。

关键词:遥感;Penman-Monteith;蒸散发;土壤含水量

中图分类号:TV11 **文献标志码:**A **开放科学(资源服务)标志码(OSID):**

蒸散发是地表能量平衡与水量平衡的重要组成部分[1],是连接地表陆气水分交换的中间环节,同时,蒸散发也是农业用水管理中的重要要素。因此,实现蒸散发的准确模拟,对加强水资源管理[2]、实现水资源高效利用[3]有积极意义。

传统的蒸散发观测以地面站点观测为主[4],但无法获取大尺度上的蒸散发时空分布。遥感技术的不断发展,为大尺度的蒸散发监测提供了技术手段[5],主要包括基于能量平衡原理的余项法[6-7]和基于彭曼公式的物理模型法[2]两大类。其中,基于彭曼公式的物理模型法利用 P-M 模型直接对蒸散发估算,便于利用大尺度的地面遥感数据[8]。由 Cleugh 提出[9]、并由 Mu 等[10]进行改进的基于叶面指数的遥感彭曼模型(遥感 P-M)是这类方法的典型代表。

遥感 P-M 模型以彭曼公式为基础,是一种通过对地表导度 G_s 进行参数化,来直接推求蒸散发的方法。该方法通过对冠层结构进行概化,在植被冠层郁闭的情况下可取得较高的估算精度[11],当植被稀疏时,可通过对表面阻抗进行参数化来改善模拟效果。在该模型的应用过程中,众多学者又对模型做了进一步完善。Mu 等[10]通过引入叶面指数和气象要素改善了地表导度的计算,满足了利用多站点观测数据进行验证的需求。Leuning 等[12]在此基础上发展了具有生物物理基础的模型,又称为“PML”模型,Zhang[13]和李红霞[14]基于此模型在澳大利亚地区进行了蒸散发的模拟,王海波等[11]也利用该模型对我国黑河流域的蒸散发进行了分析。这些研究使遥感 P-M 模型中地表导度的参数化方案有了长足发展,并使该模型成为开展全球尺度地表蒸散发模拟和监测的重要手段[15],同时也为本研究实现蒸散发的准确模拟奠定了基础。

虽然遥感 P-M 模型已在全球范围内的不同气

收稿日期:2019-04-01 **修回日期:**2019-10-30 **网络出版时间:**2019-11-20
网络出版地址:http://kns.cnki.net/kcms/detail/13.1334.TV.20191119.1653.002.html
基金项目:国家重点研发计划(2017YFC0405803)

作者简介:段浩(1989—),男,河北定州人,工程师,博士,主要从事遥感水文及数据同化方面研究。E-mail:dhao@iwhr.com

候和植被覆盖区得到应用,但对该模型的应用主要围绕改善蒸散发的模拟精度展开,而分析下垫面其他要素变化对该模型产生影响的研究较少,仅有的研究是 Zhang 等[15]基于遥感 P-M 模型分析了气候条件对土壤蒸发和植被蒸腾的影响。土壤含水量的变化对蒸散发的模拟影响显著,王朝华的相关研究表明,华北地区 0.3 m 以上耕作层蒸散发量可达到总蒸散发的 76%以上[16]。但基于遥感蒸散发模型分析地表土壤含水量变化对土壤蒸发和植被散发影响的研究并不多见。本文以华北平原望都观测站为研究对象,以涡度相关观测和地表土壤含水量遥感监测产品为基础,研究地表蒸散发过程中土壤含水量变化对土壤蒸发的影响机理,以期对该模型的后续应用及土壤蒸发的计算提供参考。

1　数据与方法

1.1　数　据

此次研究所选用的望都涡度相关观测站建立于 2016 年,于 2018 年下半年开始进行涡度相关观测。该测站位于 115°6′57″E,38°42′9″N,试验占地近 2.67 hm^2,海拔 51 m,地处华北平原(图 1),属于温带季风气候区,年均气温 11.8 ℃,雨热同期。望都站有着最新的涡度相关监测和可以结合分析的遥感土壤含水量数据,同时地处华北平原,便于同对该区域的已有研究成果做对比分析。

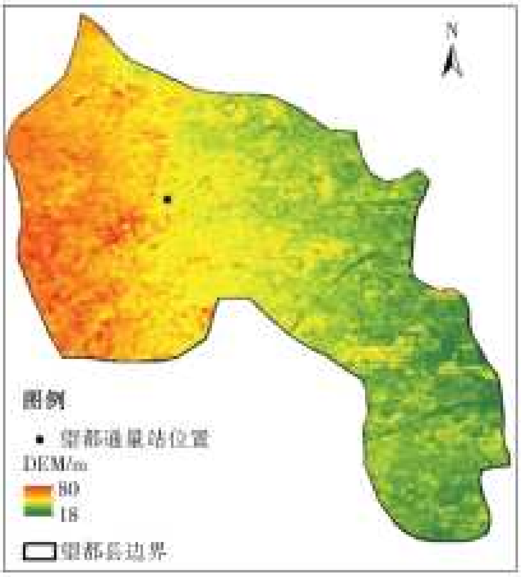

图 1　望都站位置

本研究所用数据包括望都站 2018 年 5 月至 10 月的蒸散发数据(其中 7 月份因观测问题资料缺失);气象数据,包括气温、日照时数、湿度、气压等,由国家气象信息中心发布的日数据产品(http://data.cma.cn/)插值得到;土壤含水量地面观测数据选用国家土壤墒情测报系统对望都地表 10 cm 处的土壤含水量观测数据,遥感数据选用 SMAP(the soil moisture passive and active)土壤含水量数据的 L4 级产品,SMAP 土壤含水量产品具有较高的精度[17],且已得到较多应用;观测站的土地利用以耕地为主。

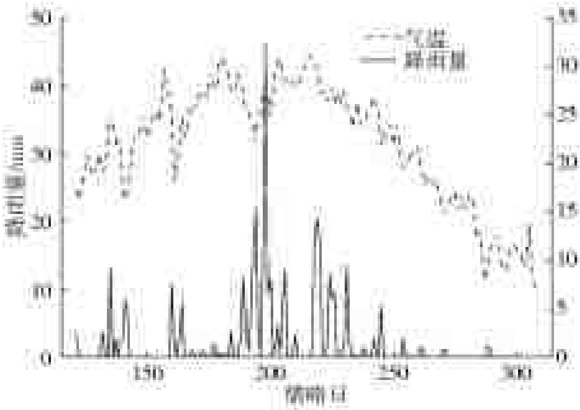

图 2　望都站 2018 年 5 月至 10 月降雨和气温变化

1.2　方　法

1.2.1　蒸散发反演模型

利用遥感 P-M 模型估算蒸散发在开放水面和湿润下垫面的潜在蒸发计算方法基础上发展而来[11],基本思想是引入"表面阻抗"[18]的概念,得到非饱和下垫面蒸散发的 P-M 公式,基本计算过程为[12]

$$\lambda E=\frac{\varepsilon A+(\rho_a c_p/\gamma)D_a G_a}{\varepsilon+1+G_a/G_s} \tag{1}$$

式中:E 是蒸散发;λ 指汽化潜热;ε 是温度-饱和水汽压曲线斜率与干湿表常数的比值;ρ_a 是空气密度;C_p 是空气定压比热;D_a 是参考高度饱和水汽压差;A 是可用能量,为净辐射与土壤热通量的差值;G_a 是空气动力学导度;G_s 是地表导度。

在计算中,该方法将蒸散发分为土壤蒸发(E_c)和植被蒸腾(E_s)两部分进行计算[12],基本思路是将可用能量的吸收分解为冠层吸收和土壤吸收两部分[14]。具体表示为

$$\lambda E=E_s+E_c=\frac{\varepsilon A_c+(\rho_a c_p/\gamma)D_a G_a}{\varepsilon+1+G_a/G_c}+\frac{f\varepsilon A_s}{\varepsilon+1} \tag{2}$$

式中:f 是土壤蒸散发系数;A_c 和 A_s 分别是可用能量中被冠层和土壤吸收的部分,且被土壤吸收的能量占可用能量的 τ 倍,τ 可通过叶面积指数 LAI 的经验关系得到。

冠层导度 G_c 可根据冠层上方叶面最大气孔导度 g_{sx} 和 LAI 的关系得到,为

$$G_c=\frac{g_{sx}}{k_Q}\ln\left[\frac{Q_h+Q_{50}}{Q_h\exp(-k_A\cdot \mathrm{LAI})+Q_{50}}\right]\left[\frac{1}{1+\frac{D_a}{D_{50}}}\right] \tag{3}$$

式中：k_Q 是短波辐射衰减系数，常取 0.6；k_A 是可用辐射衰减系数，取值 0.6；Q_h 是冠层上方的可见光辐射通量；Q_{50} 和 D_{50} 是当气孔导度 $g_s = g_{sx}/2$（g_{sx} 是 g_s 的最大值）时的可见光辐射通量和水汽压差，通常取值分别为 2.6 MJ/(m² · d)和 0.8 kPa。

通常情况下，在日尺度的蒸散发模拟过程中，蒸散发量对空气动力学导度的敏感性较弱[19]，因此可在高空间分辨率的气象数据不完备时，按照地物不同对 G_a 赋值[13]。净辐射 R_n 根据地表反照率、太阳短波辐射及净长波辐射得到，汽化潜热(λ)、干湿表常数(γ)等气象参数按相应公式进行计算，具体可参考文献[20]和[21]，这两篇文献中给出了计算蒸散发所需气象要素各分量的步骤。

除相对不敏感的参数外，利用遥感 P-M 模型模拟蒸散发需率定的参数为 f 和 g_{sx}，率定过程常根据模拟与实测蒸散发确定 Nash-Sutcliffe 系数[22] (NSE)确定，通过优化算法进行参数率定。其中，f 越大表明研究区的土壤状况越湿润，而 g_{sx} 的取值与研究区的植被类型相关[23]。

1.2.2　土壤蒸发与地表土壤含水量关系分析

为深入分析不同土壤湿度条件对遥感 P-M 模型反演蒸散发过程中土壤蒸发系数 f 的影响，此次研究根据模拟时段内土壤湿度的观测情况，依据土壤含水量大小将模拟时段划分为 3 个阶段，分别对不同阶段的蒸散发过程进行参数率定。在此基础上，将各阶段 f 的率定结果与相应时期土壤含水量进行对比，分析土壤湿度变化对遥感 P-M 模型参数率定的影响。同时，对各个阶段的土壤蒸发和植被散发进行汇总，分析地表土壤含水量变化对土壤蒸发的影响。

1.2.3　遥感 P-M 模型参数不确定性分析

为分析模型参数率定结果的不确定性，采用 GLUE (generalized likelihood uncertainty estimation) 方法[24]进行参数的不确定性分析，该方法认为模拟值与实测值越接近，二者的似然度越大，当模拟值与实测值的差值大于规定的阈值时，似然度为 0。GLUE 算法的计算过程如下：

确定似然度函数。似然度函数用来反映模型模拟值与观测值之间的差异，确定性系数(R^2)是常用的表现形式之一，其表达式为

$$L(\theta_i|Y)=1-\frac{\sum_{i=1}^{n}(ET_{\mathrm{obs},i}-ET_{\mathrm{sim},i})^2}{\sum_{i=1}^{n}(ET_{\mathrm{obs},i}-ET_{\mathrm{mean}})^2} \tag{4}$$

式中：θ_i 是第 i 组参数；Y 为参数组取值；L 为似然值，此研究中为 R^2；$ET_{\mathrm{obs},i}$ 为第 i 组参数的观测值，$ET_{\mathrm{sim},i}$ 为模拟值，ET_{mean} 为观测值的均值。

参数概率分布。通常参数的先验分布难以确定，通常采用均匀分布的方式来描述，本文利用均匀分布来描述遥感 P-M 模型中的 f 和 g_{sx} 两个参数的先验分布。

分析不确定性。似然度低于阈值的，认为似然度为 0。本研究中，似然函数的阈值设置为 0.5。

为分析模型参数的不确定性区间，本研究选用常用的 3 种指标进行分析，分别是 CR(containing ratio)、B(average band-width)及 S(average asymmetry degree)。3 类指标的含义及计算方法如下。

CR 代表不确定性区间内的观测样本占总样本的比例，其表达式为

$$\mathrm{CR}=\frac{n_{ET_{in}}}{n}\times 100\% \tag{5}$$

式中：$n_{ET_{in}}$ 是不确定性区间内观测样本的数量；n 是观测样本的总数。

B 是指在模拟期内，模拟值的最大值和最小值之差的平均宽度，其表达式为

$$B=\frac{\sum_{i=1}^{n}(ET_{\mathrm{upper},i}-ET_{\mathrm{lower},i})}{n} \tag{6}$$

式中：$ET_{\mathrm{upper},i}$ 和 $ET_{\mathrm{lower},i}$ 是在第 i 个模拟时刻，不确定性区间上模拟值的最大和最小值。

S 用来表征不确定性区间的分布与观测值的对称情况，其计算过程为

$$S=\frac{\sum_{i=1}^{n}|(ET_{\mathrm{upper},i}-ET_i)/(ET_{\mathrm{upper},i}-ET_{\mathrm{lower},i})-0.5|}{n} \tag{7}$$

式中：ET_i 是第 i 个计算时刻的观测值。

2　结果与讨论

2.1　模型率定及模拟结果

利用遥感资料、气象数据及遥感 P-M 模型，基于模拟退火算法[25]，对 2018 年望都站的蒸散发过程进行模型参数估计，其中以 10 月为验证期，5 至 9 月为率定期。经过参数率定，望都站的由涡度相关观测得到的蒸散发与模拟值间的 NSE 为 0.559，表明遥感 P-M 模型在望都站的模拟具有较好的精度。f 的率定值为 0.886，表明在该时段内望都站的土壤整体上较为湿润；g_{sx} 的率定结果是 0.046。

望都站遥感 P-M 蒸散发的模拟值与观测值的散点对比情况见图 3，散点图的相关系数为 0.562 1，且线性拟合结果与 1∶1 线较接近，表明反演值与实测值间具有较好的相关性。

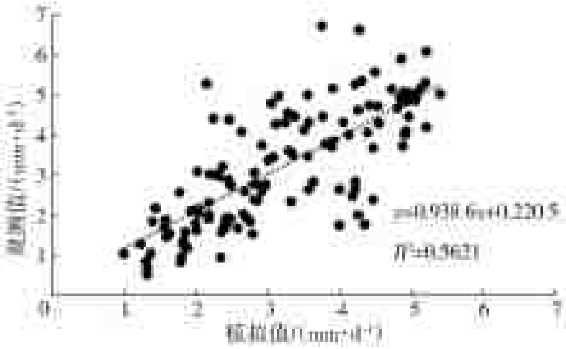

图 3　望都站 2018 年 5 月至 10 月蒸散发实测与模拟值对比

2.2　土壤含水量变化对参数率定的影响

由于土壤墒情测报系统中，望都站的监测为每 10 天上报一次，因此土壤含水量的实测值无法形成逐日的序列。本文选用土壤湿度主-被动探测卫星(SMAP)地表土壤含水量数据作为评估望都站地区地表土壤水分变化的参考，首先对墒情测报系统中观测日的土壤含水量(10 cm 深度)与 SMAP 数据进行对比，验证 SMAP 数据产品的有效性。从图 4(a)可以看出，SMAP 土壤含水量产品与实测值具有一定的一致性，Pearson 相关系数为 0.48，均方根误差为 0.05 cm^3/cm^3，考虑到 SMAP 为大尺度微波观测的数据产品，该误差在可接受的范围内[26]。图 4(b)则进一步表明 SMAP 数据虽整体上比实测值偏低，但能体现地表土壤含水量的变化趋势。SMAP 与实测土壤含水量的散点拟合精度不高，一方面是因微波只能观测近地表的土壤水分，而此处将 SMAP 数据视为地表 10 cm 处土壤含水量的近似；另一方面 SMAP 数据空间分辨率为 9 km，将墒情站所在网格的 SMAP 数据与观测值对比，实际是取 9 km×9 km 网格的平均，具有不确定性。同时，望都站降雨与 SMAP 数据的对比(图 5)进一步显示，SMAP 数据的变化与降雨量的起伏基本一致。因此，本文利用 SMAP 地表土壤含水量产品来表征望都站实际土壤含水量的变化特征。

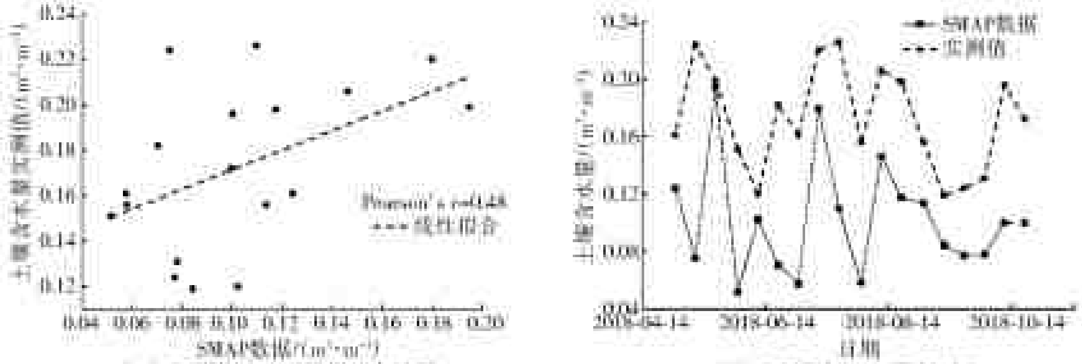

(a) 实测值与SMAP数据拟合结果　　(b) 实测值与SMAP数据对比

图 4　望都站 2018 年 5 月至 10 月土壤含水量实测值与 SMAP 数据拟合及对比

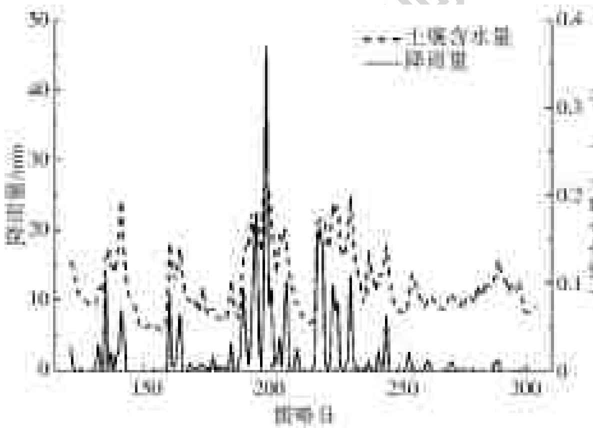

图 5　望都站 SMAP 土壤含水量与降雨对比

将研究时段根据 SMAP 地表土壤湿度的大小按升序排列并做 3 等分，分别命名为阶段 1、阶段 2 和阶段 3，每个阶段 60 天左右(代表 60 个观测值)，3 个阶段的土壤含水量最小值为 0.044 7 cm^3/cm^3，最大值为 0.212 5 cm^3/cm^3，3 个阶段的临界值分别为 0.076 8 cm^3/cm^3 和 0.106 4 cm^3/cm^3，即阶段越高，土壤含水量值越大。依次对 3 个阶段、不同土壤湿度条件下的蒸散发进行遥感 P-M 模型的敏感参数率定和蒸散发模拟，结果见表 1。率定结果显示，按照 SMAP 土壤含水量产品对研究时段进行划分，土壤蒸发系数 f 的率定结果均较大，表明在模拟期内研究区的土壤整体较为湿润，其中，又以阶段 3 的土壤蒸发系数最大。但在阶段 2，遥感 P-M 模型得到的土壤蒸发系数 0.78 要小于阶段 1 的结果 0.88，表明模型在模拟期内的土壤蒸发系数与地表土壤含水量不是简单的线性相关，模型率定结果具有一定不确定性。

表 1　分阶段参数率定结果

土壤含水量区间	参数率定结果	
	f	g_{sx}
阶段 1	0.883 9	0.009 7
阶段 2	0.782 9	0.043 3
阶段 3	1	0.050 0

造成参数率定结果不确定性的原因是多方面的。首先是优化算法方面,本文采用模拟退火算法对遥感 P-M 的敏感参数进行率定,初始种群个数设为 50,最大迭代次数设为 20,算法中不同参数的选取,都有可能对参数率定的结果产生影响。其次,SMAP 地表土壤含水量的数据精度会对阶段划分产生影响。最后,敏感参数区间的选取也会影响参数率定的结果,综合已有相关研究成果,本文 f 和 g_{sx}的区间分别为[0.050,1.000]和[0.002,0.050]。

2.3　土壤含水量变化与蒸发量的关系

为进一步分析不同地表土壤含水量值对土壤蒸发的影响,利用 2.1 小节中望都站的参数率定结果计算各阶段的土壤蒸发和植被散发量。望都站的主要作物为冬小麦和夏玉米,但因本研究中的阶段划分以土壤含水量大小为依据,同一分段可能包含不同季节的日期,因此本小节主要从土壤含水量大小的角度分析其与蒸发的关系。图 6(a)给出了不同分段时期内土壤蒸发量的对比情况,其中横轴为各阶段内按 SMAP 土壤含水量由低到高排序生成的序号(不包含无蒸散发观测日期和遥感数据为无效值的日期)。按照土壤含水量大小划分不同阶段,目的是更直观地分析在不同土壤含水量条件下土壤蒸发和植被散发的变化情况。从 3 个阶段划分来看,地表土壤含水量越大,土壤蒸发量越大。这种现象在阶段 1 体现的较为明显,阶段 1 的土壤含水量整体最低,在 3 个阶段中土壤蒸发量也偏低,从各个阶段的日均土壤蒸发量来看(表 2),阶段 1 的日均土壤蒸发 0.139 6 mm/d 也是 3 个阶段中最低的。这是由于土壤蒸发主要是土壤的失水过程,而 0～20 cm 是土壤蒸发强烈影响的土层,土壤供水条件良好时,土壤水分会充分进行蒸发,当土壤含水量小于田间持水量时,随着毛管连续状态的破坏,土壤蒸发量也逐渐降低[27]。

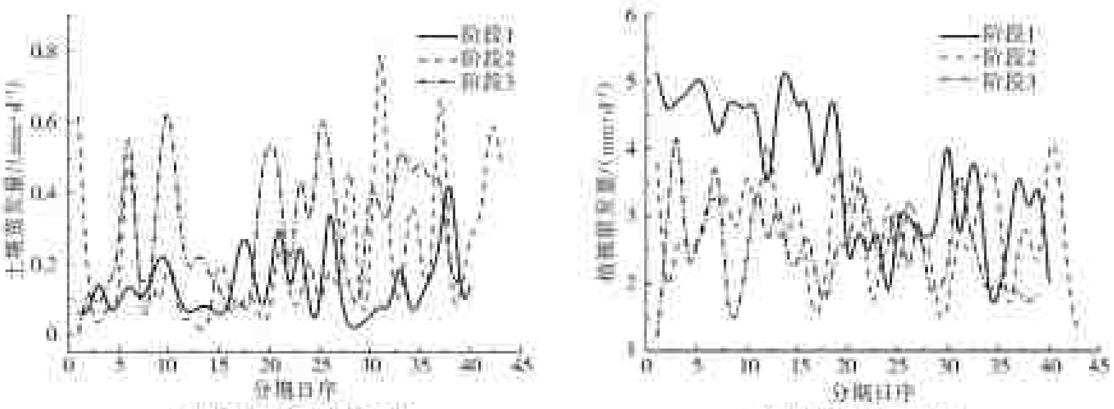

(a) 模拟土壤蒸发量变化　(b) 植被散发量变化

图 6　望都站 2018 年 5 月至 10 月分阶段模拟土壤蒸发量和植被散发量变化

表 2　不同阶段土壤蒸发和植被散发均值统计

土壤含水量区间	土壤含水量范围/(cm³·cm⁻³)	土壤蒸发均值/(mm·d⁻¹)	植被散发均值/(mm·d⁻¹)
阶段 1	(0.044 7,0.076 8)	0.139 6	3.652 1
阶段 2	(0.076 8,0.106 4)	0.221 9	2.754 9
阶段 3	(0.106 4,0.212 5)	0.297 9	2.509 4

在本研究选取的模拟期内,地表土壤含水量的大小与植被散发变化的相关性则较差。从图 6(b)可以看出,在 SMAP 土壤含水量最低的阶段 1,植被散发的模拟结果在很多模拟日是最高的,尤其是在阶段 1 的前 20 个模拟日。除土壤含水量外,植被散发还会受温度、日照、植物生理特性等因素的影响。由于本研究按 SMAP 地表土壤含水量的大小对模拟期分段,使生长期在各分段内不连续,且在阶段划分时未考虑气象条件,导致植被散发量的变化特征不明显。

如前文所述,地表 0～20 cm 的土层为土壤蒸发强烈的土层,但受遥感观测深度的限制,本文选取的 SMAP 微波产品无法反映 20 cm 深度的土壤水分状况,只作为地表 10 cm 处土壤含水量的近似。因此,本研究的分析只针对地表土壤含水量的变化对蒸散发的影响进行,而对 10～20 cm 深度的土壤含水量与蒸散发的关系分析,可基于土壤含水量的同化产品(如 GLDAS 等)展开,相关工作将在后续的研究中进行。

2.4　模型参数的不确定性分析

为进一步对模型参数的不确定性进行分析,本研究基于 GLUE 算法进行了参数选取对模拟结果影响的分析。对 f 和 g_{sx}参数按照蒙特卡洛方法进行取值,共取样10 000次。图 7 给出了两种敏感参数的取值与似然函数值大于阈值的结果对比情况。从中可以看出,参数 f 和 g_{sx}均服从指数分布,f 的

取值区间集中在 0.78～0.99；g_{sx} 的取值越大，模型得到较高似然值的概率越大。相比而言，参数 f 对模型的不确定性更大。对模型 3 种不确定性指标的结果显示，CR 值为 32，B 值为 0.63(mm/d)，S 值是 1.25，蒸散发模拟值与不确定性区间的相互关系(图 8)也显示，一部分模拟值位于不确定性区间之外(图中蒸散发中断部分为监测缺失日期)，因此模型参数具有不确定性[28]。

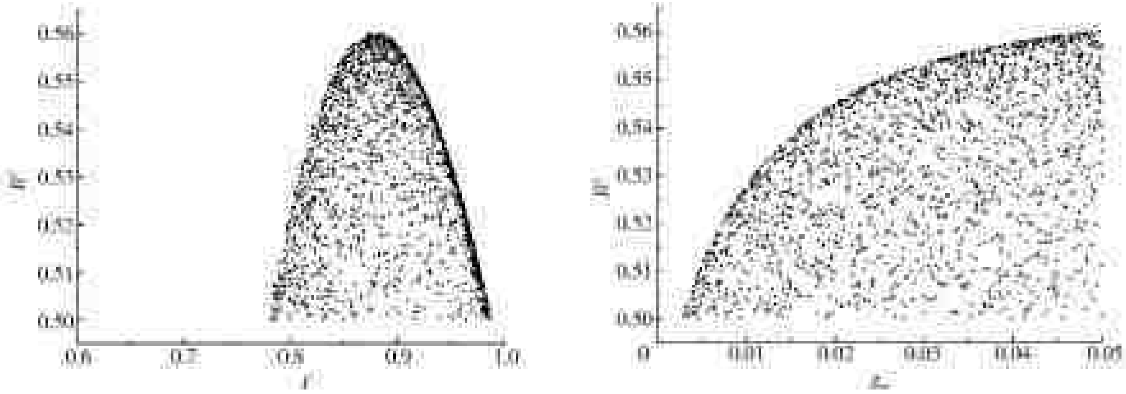

图 7　敏感参数与似然值对比散点

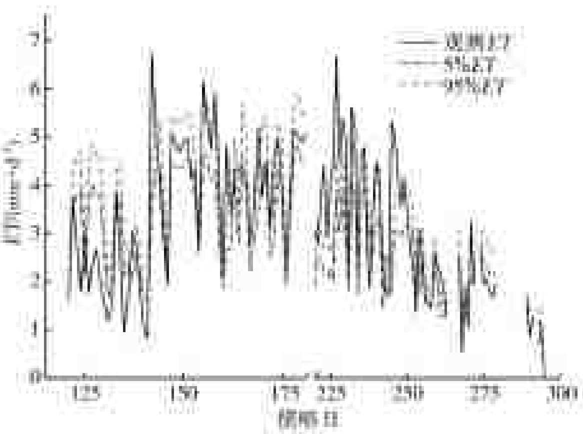

图 8　望都站日蒸散发模拟不确定性区间

总体上，遥感 P-M 模型较好地模拟了望都站的蒸散发变化过程，具有较高的模拟精度。但是受模型参数的先验分布选取规则、模型结构、采样规则、输入数据误差等因素的影响，模拟过程仍存在一定的不确定性，模型并未能完全模拟蒸散发的变化过程。

3　结　论

本文利用遥感 P-M 模型对望都站 5 至 10 月的蒸散发进行了反演，并结合 SMAP 地表土壤含水量产品分析了地表土壤含水量变化对模型参数率定及土壤蒸发和植被散发的影响，主要得出以下结论。

(1)基于遥感 P-M 模型对望都站 2018 年 5 至 10 月的蒸散发进行模拟，模拟值与实测值的 NSE 系数为 0.56，该方法对望都站的蒸散发具有较好的模拟能力。

(2)遥感 P-M 模型在地表土壤含水量最大时，土壤蒸发系数的率定结果取得最大值，但二者间仍具有不确定性。

(3)在只考虑地表土壤含水量变化的情况下，土壤含水量大小与土壤蒸发量的一致性较为明显，而受到气象条件、植被生育期等因素的影响，土壤含水量与植被散发量间一致性较弱。

(4)对模型参数率定的不确定性分析表明，虽然模拟得到的蒸散发结果能较好地反应实际观测情况，但遥感 P-M 模型具有一定的不确定性，敏感参数中 f 的不确定性更大。

参考文献：

[1]　李放，沈彦俊. 地表遥感蒸散发模型研究进展[J]. 资源科学，2014，36(7)：1478-1488. DOI：1007-7588(2014)07-1478-11.

[2]　辛晓洲，田国良，柳钦火. 地表蒸散定量遥感的研究进展[J]. 遥感学报，2003，7(3)：233-240. DOI：1007-4619(2003)03-0233-08.

[3]　张发耀，王福民，周斌，等. 基于 SEBAL 模型的浙江省区域蒸散发量估算研究[J]. 人民长江，2013，44(17)：40-44. DOI：1001-4179(2013)17-0040-05.

[4]　冯景泽，王忠静. 遥感蒸散发模型研究进展综述[J]. 水利学报，2012，43(8)：914-925. DOI：0559-9350(2012)08-0914-12.

[5]　王娅娟，孙丹峰. 基于遥感的区域蒸散研究进展[J]. 农业工程学报，2005，21(7)：162-167. DOI：1002-6819(2005)07-0162-06.

[6]　SU Z. The surface energy balance system (SEBS) for estimation of turbulent heat fluxes[J]. Hydrology and Earth System Sciences，2002，6(1)：85-99. DOI：10.5194/hess-6-85-2002.

[7]　BASTIAANSSEN W G M，MENENTI M，FEDDES R A，et al. A remote sensing surface energy balance algorithm for land (SEBAL)-1. Formulation[J]. Journal of

Hydrology,1998,212(1-4):198-212. DOI:10.1016/S0022-1694(98)00253-4.

[8] GUO X Y,CHENG G D. Advances in the application of remote sensing to evapotranspiration research in arid regions[J]. Advances in Earth Science,2011,26(8):848-858. DOI:10.11867/j.issn.1001-8166.2011.08.0848.

[9] CLEUGH H A,LEUNING R,MU Q Z,et al. Regional evaporation estimates from flux tower and MODIS satellite data[J]. Remote Sensing of Environment,2007,106:285-304. DOI:10.1016/j.rse.2006.07.007.

[10] MU Q Z,HEINSCH F A,ZHAO M S,et al. Development of a global evapotranspiration algorithm based on MODIS and global meteorology data[J]. Remote Sensing of Environment,2007,111,519-536. DOI:10.1016./j.rse.2007.04.015.

[11] 王海波,马明国. 基于遥感和 Penman-Monteith 模型的内陆河流域不同生态系统蒸散发估算[J]. 生态学报,2014,34(19):5617-5626. DOI:10.5846/stxb201301150102.

[12] LEUNING R,ZHANG Y Q,RAJAUD A,et al. A simple surface conductance model to estimate regional evaporation using MODIS leaf area index and the Penman-Monteith equation[J]. Water Resources Research,2008,44,W10419. DOI:10.1029/2007WR006562.

[13] ZHANG Y Q,CHIEW F H S,ZHANG R,et al. Estimating catchment evaporation and runoff using MODIS leaf area index and the Penman-Monteith equation[J]. Water Resources Research,2008,44(10),DOI:10.1029/2007wr006563.

[14] 李红霞,张永强,张新华,等. 遥感 Penman-Monteith 模型对区域蒸散发的估算[J]. 武汉大学学报(工学版),2011,44(4):457-461. DOI:1671-8844(2011)04-0457-05.

[15] ZHANG Y Q,CHIEW F H S,PENA-ARANCIBIA J,et al. Global variation of transpiration and soil evaporation and the role of their major climate drivers[J]. Journal of Geophysical Research:Atmospheres,2017,122,6868-6881. DOI:10.1002/2017JD027025.

[16] 王朝华. 农田蒸散发量变化规律分析[J]. 水文,2005,25(3):35-37. DOI:1000-0852(2005)03-0035-03.

[17] CHAN S K,BINDLISH R,E. O'NEILL P,et al. Assessment of the SMAP passive soil moisture product[J]. IEEE Transactions on Geoscience and Remote Sensing,2016,54(8):4994-5007. DOI:10.1109/tgrs.2016.2561938.

[18] MONTEITH J L. Evaporation and environment//The State and Movement of Water in Living Organisms. Symposium of the Society for Experimental Biology[M]. England:Cambridge University Press,1965,19:205-234.

[19] LEUNING R. A critical appraisal of a combined stomatal-photosynthesis model for C3 plants[J]. Plant,Cell and Environment,1995(18):339-355. DOI:10.1111/j.1365-3040.1995.tb00370.x.

[20] ALLEN R G,PEREIRA L S,RAES D,et al. Crop evapotranspiration:Guideline for computing crop requirement[S]. Irrigation and Drainage,Rome,Italy,1998,FAO.

[21] 朱仲元. 干旱半干旱地区天然植被蒸散发模型与植被需水量研究[D]. 呼和浩特:内蒙古农业大学,2005.

[22] NASH J E,SUTCLIFFE J V. River forecasting using conceptual models,1. A discussion of principles[J]. 1970,97:337-351.

[23] KELLIHER F M,LEUNING R,RAUPACH M R,et al. Maximum conductances for evaporation from global vegetation types[J]. Agricultural and Forest Meteorology,1995(73):1-16.

[24] BEVEN K,BINLEY A. The future of distributed models:model calibration and uncertainty prediction[J]. Hydrological Processes,1992(6):279-298. DOI:10.1002/hyp.3360060305.

[25] 蒋美云. 基于模拟退火算法优化的 BP 神经网络预测模型[J]. 软件工程,2018,21(7):36-38. DOI:2096-1472(2018)-07-36-03.

[26] 贾艳昌,谢谟文,姜红涛. 全球 36 km 格网土壤水分逐日估算[J]. 地球信息科学学报,2017,19(6):854-860. DOI:10.3724/SP.J.1047.2017.00854.

[27] 芮孝芳. 水文学原理[M]. 北京:中国水利水电出版社,2004.

[28] WANG H J,XIAO W H,WANG Y C,et al. Assessment of the impact of climate change on hydropower potential in the Nanliujiang River basin of China[J]. Energy,2019(167):950-959. DOI:10.1016/j.energy.2018.10.159.

·译文(Translation)·

DOI:10.13476/j.cnki.nsbdqk.2020.0048

Assessment the relationship between soil evaporation and soil moisture using remote sensing Penman-Monteith model

DUAN Hao, ZHAO Hongli, JIANG Yunzhong

(China Institute of Water Resources and Hydropower Research Department of Water Resources, Beijing 100038, China)

Abstract: Soil moisture content is an important factor affecting soil evaporation. Analyzing the influence of soil moisture variation on soil evaporation has a positive effect on water resource management. The remote sensing Penman-Monteith (P-M) model is a remote sensing based method for evapotranspiration simulation and can calculate soil evaporation and vegetation transpiration separately. This study calculates the evapotranspiration for Wangdu station and investigates the effects of soil moisture on the model parameters and soil evaporation. The results showed that the model has a good performance at Wangdu station with a value of NSE (0.559). There is an uncertain relationship between soil moisture and model parameters. Comparing with the vegetation transpiration, the consistency of soil moisture and soil evaporation is stronger in the simulation period for this particular research.

Key words: remote sensing; Penman-Monteith; evapotranspiration; soil moisture

Evapotranspiration is an important component of surface energy balance and water balance[1], and it is an intermediate link connecting the surface land and air-water exchange. Simultaneously, evapotranspiration is also an important element in agricultural water management. Therefore, the accurate simulation of evapotranspiration has positive significance for strengthening water resources management[2] and realize the efficient utilization of water resources[3].

Traditional evapotranspiration observations are mainly based on ground-based station observations[4], but the large-scale spatiotemporal distribution of evapotranspiration cannot be obtained. The continuous development of remote sensing technology has provided technical means for large-scale evapotranspiration monitoring[5], which mainly includes two types of a residual method based on the principle of energy balance[6-7] and physical model method based on Penman formula[2]. Among them, the physical model based on Penman′s formula uses the P-M model to directly estimate evapotranspiration, which is convenient for using large-scale in situ remote sensing data[8]. The leaf surface index-based remote sensing Penman model (remote sensing P-M) proposed by Cleugh[9] and improved by Mu et al.[10] is a typical representative of such methods.

The remote sensing P-M model based on Penman′s formula is a direct method to calculate evap-

Received: 2019-04-01 **Revised**: 2019-10-30 **Online publishing**: 2019-11-20
Online publishing address: http://kns.cnki.net/kcms/detail/13.1334.TV.20191119.1653.002.html
Fund: National Key Research and Development Program of China (2017YFC0405803)
Author brief: DUAN Hao (1989-), male, Dingzhou, Hebei Province, engineer, Ph.D., mainly engaged in remote sensing hydrology and data assimilation research. E-mail: dhao@iwhr.com

otranspiration by parameterizing the surface conductance G_s. By generalizing the canopy structure, this method can obtain high estimation accuracy[11] when the canopy is closed. The surface impedance can be parameterized to improve the simulation effect when the vegetation is sparse. During application process of this model, many scholars have further improved the model. Mu et al. improved the calculation of surface conductance by introducing foliar indices and meteorological elements and met the need of verification using multi-site observation data. Leung et al. [12] developed a model with a biophysical basis, also known as the "PML" model. Zhang[13] and Li Hongxia[14] performed evapotranspiration simulations in Australia based on the PML model. Wang Haibo et al. [11] also used this model to analyze the evapotranspiration of the Heihe River basin in China. These studies have made great progress in the parameterization scheme of the surface conductance in the remote sensing PM model and made the model an important method for the simulation and monitoring of surface evapotranspiration on a global scale[15], which also laid a foundation for the accurate simulation of evapotranspiration in this study.

Even though the remote sensing PM model has been applied in different climate and vegetation coverage areas around the world. The application of the model is mainly focused on improving the simulation accuracy of evapotranspiration, and analyzing the impact of changes in other factors on the underlying surface on the model. Sole research of Zhang et al. [15] analyzed the effects of climatic conditions on soil evaporation and vegetation transpiration based on remote sensing PM models. The change in soil water content has a significant impact on the simulation of evapotranspiration. The related research by Wang Chaohua shows that the evapotranspiration of the cultivated layer above 0.3 m in North China can reach more than 76% of the total evapotranspiration[16]. However, there are few studies on the effects of surface soil moisture changes on soil evaporation and vegetation emission based on remote sensing evapotranspiration models. In this paper, Wangdu observation station in North China Plain is taken as the research object, and studies the effect of soil water content changes on soil evaporation during evapotranspiration based on eddy-covariance observations and remote sensing monitoring products of surface soil water content, in order to provide a reference for the subsequent application of the model and the calculation of soil evaporation.

1 Data and methods

1.1 Data

The Wangdu observation station selected by the research institute was established in 2016 and began to carry out eddy-covariance observation in the second half of 2018. The station is located at 115°6′57″ E, 38° 42′9″ N, covering an area of nearly 2.67 hm^2 at an altitude of 51 m. It is located in the North China Plain (Fig. 1) and belongs to the temperate monsoon climate zone with an average annual temperature of 11.8 ℃. Wangdu station has the latest eddy-covariance monitoring and remote sensing soil moisture data that can be combined with the analysis, which is convenient for comparison and analysis with existing research results in the region.

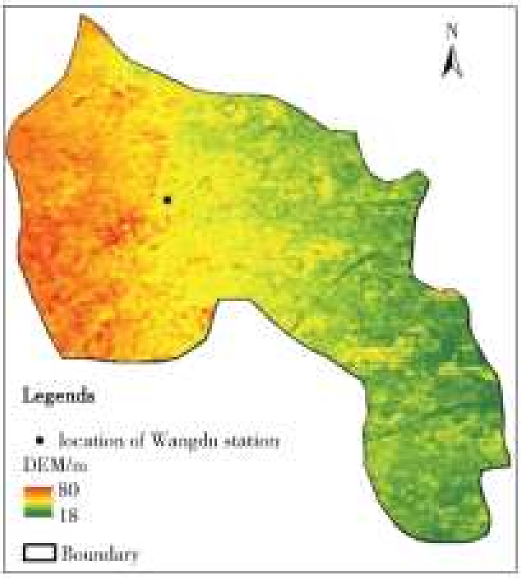

Fig. 1　The location of Wangdu station

In this study meteorological data such as air temperature, sunshine hours, humidity, pressure included the evapotranspiration data of Wangdu station from May to October 2018 (lack of missing observations in July)(Fig. 2). The daily data product obtained by the interpolation method is issued by the National Meteorological Information Center (http://data. cma. cn/). The ground observation data of soil moisture content is selected from the national soil moisture measurement and prediction system for the observation data of soil moisture content at 10cm of the Wangdu surface. The L4 product of SMAP (Soil Moisture Passive and Active) soil moisture data is selected as the remote sensing data. The SMAP soil moisture product has a high accuracy[17] and has been widely used. The land use in the observation station is mainly cultivated land.

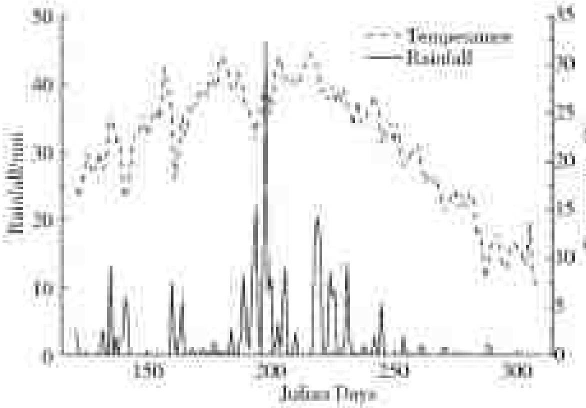

Fig. 2 Precipitation and temperature change at Wangdu station from May to October in 2018

1.2 Methods

1.2.1 Evapotranspiration inversion model

A remote sensing PM model was developed based on the calculation method of potential evapotranspiration from open water and wet underlying surfaces[11]. The basic idea is to introduce the concept of "surface impedance"[18] to obtain the P-M formula of unsaturated underlying evapotranspiration, the basic calculation process is[12]

$$\lambda E=\frac{\varepsilon A+(\rho_a c_p/\gamma)D_a G_a}{\varepsilon+1+G_a/G_s} \tag{1}$$

where E is the evapotranspiration; λ is the latent heat of vaporization; ε is the ratio of the slope of the temperature saturated vapor pressure curve to the dry-wet surface constant; ρ_a is the air density; c_p is the specific heat of constant air pressure; D_a is the differential pressure of the saturated vapor at the reference height; A is the available energy, which is the difference between the net radiation and the soil heat flux; G_a is the aerodynamic conductivity; G_s is the surface conductance.

In calculation, the evapotranspiration is divided into two parts, soil evaporation (E_c) and vegetation transpiration (E_s)[12]. The basic idea is to decompose the absorption of available energy into canopy absorption and soil absorption[14]. Specifically expressed as

$$\lambda E=E_s+E_c=\frac{\varepsilon A_c+(\rho_a c_p/\gamma)D_a G_a}{\varepsilon+1+G_a/G_c}+\frac{f\varepsilon A_s}{\varepsilon+1} \tag{2}$$

where f is the soil evapotranspiration coefficient; A_c and A_s are the parts of available energy absorbed by the canopy and soil respectively, and the energy absorbed by the soil accounts for τ times of available energy, τ can be obtained through the empirical relationship of LAI.

The canopy conductance, G_c, can be obtained from the relationship between the maximum stomatal conductance, g_{sx}, and LAI

$$G_c=\frac{g_{sx}}{k_Q}\ln\left[\frac{Q_h+Q_{50}}{Q_h\exp(-k_A\cdot\mathrm{LAI})+Q_{50}}\right]\left[\frac{1}{1+\frac{D_a}{D_{50}}}\right] \tag{3}$$

where k_Q is the short wave radiation attenuation, usually 0.6; k_A is the available radiation attenuation coefficient, taken as 0.6; Q_h is the visible radiation flux above the canopy; Q_{50} and D_{50} are the visible radiation flux and water vapor pressure difference when the stomatal conductance $g_s=g_{sx}/2$ (g_{sx} is the maximum value of g_s), usually 2.6 MJ/(m^2 • d) and 0.8 kPa, respectively.

In general, the sensitivity of evapotranspiration to aerodynamic conductance is weak in the process of daily scale evapotranspiration simulation[19]. Therefore, when the meteorological data with the high spatial resolution is incomplete, the value of G_a can be assigned according to different features[13]. The net radiation R_n is obtained from the surface albedo, solar shortwave radiation, and net long-wave radiation. The meteorological parameters such as vaporization latent heat (λ), dry and wet surface constant (γ) are calculated according to the corresponding formula. For details, please refer to [20] and [21] to calculate the components of meteorological elements required for vaporization and emission.

In addition to the relatively insensitive parameters, the remote sensing P-M model is used to simulate the evapotranspiration parameters f and g_{sx}, and the Nash Sutcliffe coefficient (NSE)[22] is usually determined according to the simulated and measured evapotranspiration. The parameters are calibrated by the optimization algorithm. Among them, the larger f is the wetter soil condition and the value of g_{sx} is related to the vegetation type in the study area[23].

1.2.2 Analysis of the relationship between soil evaporation and surface soil water content

In order to deeply analyze the influence of different soil moisture conditions on the soil evaporation coefficient f during the inversion of evapotranspiration using a remote sensing P-M model, this study divided the simulation period into 3 stages based on the observations of soil moisture during the simulation period and the soil moisture content. The parameters of different stages of the evapotranspiration process are calibrated. On this basis, the calibration results of each stage f are compared with the corresponding soil moisture content, and the effect of soil moisture changes on the calibration of remote sensing P-M model parameters is analyzed. Simultaneously, the soil evaporation and vegetation emission in each stage were summarized to analyze the impact of the change of soil moisture content on soil evaporation.

1.2.3 Uncertainty analysis of remote sensing P-M model parametersP

In order to analyze the uncertainty of calibration results of the model parameters, the GLUE (Generalized Likelihood Uncertainty Estimation) method[24] is used to analyze the uncertainty of the parameters. The method considers that the closer the simulated value is to the measured value, the greater the likelihood degree. When the difference between the simulated value and the measured value is greater than the specified threshold value, the likelihood degree is 0. The calculation process of the GLUE algorithm is as follows:

Determine the likelihood: The likelihood function is used to reflect the difference between the simulated value and the observed value of the model. The deterministic coefficient (R^2) is one of the commonly used expressions. Its expression is

$$L(\theta_i|Y)=1-\frac{\sum_{i=1}^{n}(ET_{\mathrm{obs},i}-ET_{\mathrm{sim},i})^2}{\sum_{i=1}^{n}(ET_{\mathrm{obs},i}-ET_{\mathrm{mean}})^2} \tag{4}$$

In the formula, θ_i is the parameter of group i; Y is the value of the parameter group; L is the likelihood value in this study is R^2; $ET_{\mathrm{obs},i}$ is the observation value of group i parameter; $ET_{\mathrm{sim},i}$ is the simulation value; and ET_{mean} is the mean value of observation value.

Parameter probability distribution: In general, the prior distribution of parameters is difficult to determine, and it is usually described by the uniform distribution. In this paper, the uniform distribution is used to describe the prior distribution of f and g_{sx} parameters in the remote sensing P-M model.

Analyze the uncertainty: If the likelihood is lower than the threshold, the likelihood is considered to be 0. In this study, the threshold of the likelihood function is set to 0.5.

In order to analyze the uncertainty interval of model parameters, this study selected three commonly used indexes, namely CR (Containing ratio), B (Average bandwidth) and S (Average asymmetry degree). The meanings and calculation methods of the three types of indicators are as follows

CR represents the proportion of observation samples in the uncertainty interval to the total samples, and its expression is

$$\mathrm{CR}=\frac{n_{ET_{in}}}{n}\times 100\% \tag{5}$$

where $n_{ET_{in}}$ is the number of observation samples in the uncertainty interval; n is the total number of observation samples.

B refers to the average width of the difference between the maximum value and the minimum value of the simulation value in the simulation period, and its expression is

$$B=\frac{\sum_{i=1}^{n}(ET_{\mathrm{upper},i}-ET_{\mathrm{lower},i})}{n} \tag{6}$$

Where: $ET_{\mathrm{upper},i}$ and $ET_{\mathrm{lower},i}$ are the maximum and minimum values of simulation values in the uncertainty interval at the ith simulation time.

S is used to characterize the symmetry between the distribution of the uncertainty interval and the observed value. The calculation process is as follows

$$S=\frac{\sum_{i=1}^{n}|ET_{\mathrm{upper},i}-ET_i)/(ET_{\mathrm{upper},i}-ET_{\mathrm{lower},i})-0.5|}{n} \quad (7)$$

where ET_i is the observed value at the *ith* calculation time.

2 Results and discussion

2.1 Model calibration and simulation results

The model parameters of the evapotranspiration process of Wangdu station are estimated for October as the validation period and May to September for the year of 2018 as the calibration period using remote sensing data, meteorological data and remote sensing P-M model, based on simulated annealing algorithm[25]. After the calibration of parameters, the NSE between the observed evapotranspiration and the simulated value of Wangdu station is 0.559, which indicates that the simulation of remote sensing P-M model in Wangdu station has better accuracy. The calibration value of f is 0.886, which indicates that the soil of Wangdu station is relatively moist in this period and the calibration result of g_{sx} is 0.046, respectively.

The comparison between the scatter points of the simulated P-M evapotranspiration and the observed values at Wangdu Station are shown in Fig. 3. The correlation coefficient of the scatter plot is 0.562 1, and the linear fitting result is closer to the 1∶1 line, which indicates that there is a good correlation between the inversion value and the measured value.

2.2 Influence of changes in soil water content on calibrated parameters

The monitoring of soil moisture at Wangdu station is every 10 days, the measured values of soil water content cannot obtain on a daily sequence. In

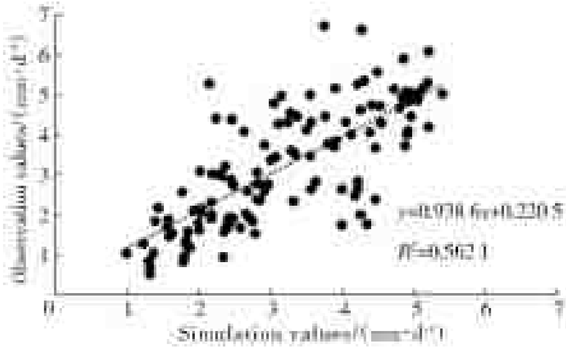

Fig. 2 Comparison of in situ and simulated evapotranspiration of Wangdu station from May to October in 2018

this paper, SMAP surface soil moisture data is used as a reference for assessing the change of surface soil moisture at Wangdu station. First, the soil moisture content (10 cm depth) of the observation day in the weather forecasting system is compared with the SMAP data to verify the validity of the SMAP data products. From Fig. 4 (a), it can be seen that the SMAP soil moisture content product has a certain consistency with the measured value. The Pearson correlation coefficient is 0.48 and the root mean square error is 0.05 cm^3/cm^3. Considering that SMAP is a large-scale microwave observation data product and the error is within the acceptable range[26]. Fig. 4 (b) further shows that although the SMAP data is lower than the measured value as a whole, it can reflect the changing trend of surface soil moisture content. The accuracy of the scatter fitting between SMAP and the measured soil moisture content is not high. On the one hand, because the microwave can only observe the soil moisture near the surface, therefore, the SMAP data is considered here as an approximation of the soil moisture content at 10 cm on the ground. The spatial resolution of the SMAP data is 9 km. Comparing the SMAP data of the grid where the Shangqing station is located with the observations, the average grid is 9 km×9 km grid which has uncertainty. Simultaneously, the comparison of rainfall and SMAP data further shows that the changes in SMAP data are consistent with the fluctuations of rainfall (Fig. 5). Therefore, this study uses SMAP surface soil moisture content products to characterize the actual soil moisture changes at Wangdu station.

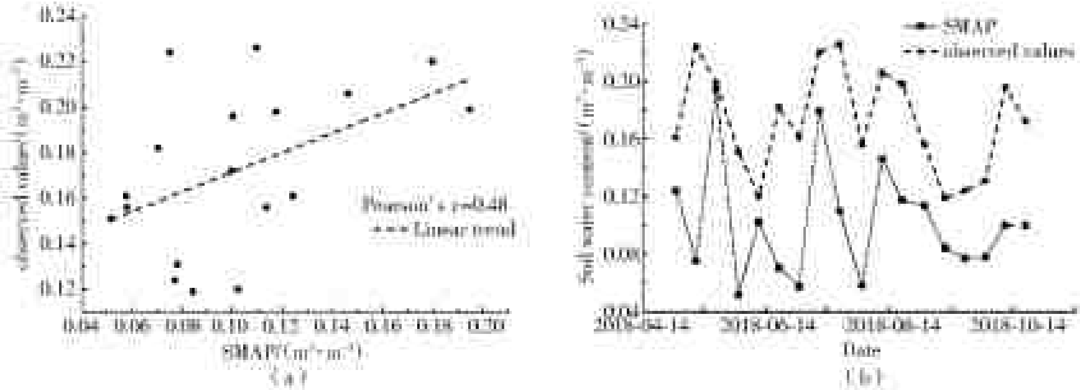

Fig. 4　Comparison of in situ and SMAP soil moisture of Wangdu station from May to October in 2018

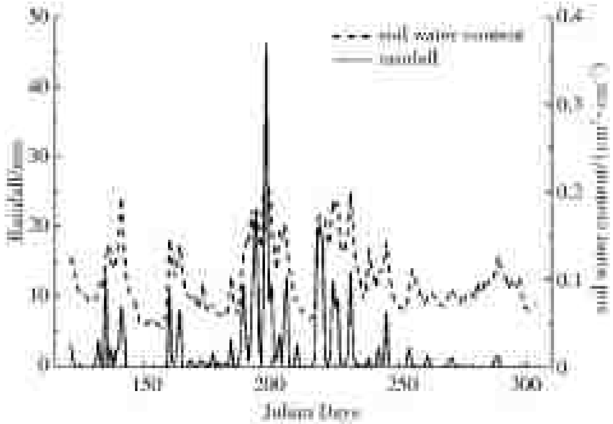

Fig. 5　Comparison of SMAP and precipitation at Wangdu station

The study period is arranged in ascending order and divided into three equal parts (stage 1, stage2, and stage3) according to the size of the soil moisture obtained from the SMAP surface. Each stage has lasted about 60 days (representing 60 observations). The minimum soil moisture content of the three stages is 0.044 7 cm^3/cm^3, the maximum is 0.212 5 cm^3/cm^3, and the critical values of the three stages are 0.076 8 cm^3/cm^3 and 0.106 4 cm^3/cm^3, respectively, suggested that higher the stage, the greater the soil water content. The evapotranspiration of three stages and different soil moisture conditions are used to calibrate the sensitive parameters of the remote sensing P-M model and simulate the evapotranspiration. The results are shown in Tab. 1. The calibration results based on SMAP soil moisture content products show that the soil evaporation coefficient f is relatively large, indicating that the soil in the study area is relatively humid during the simulation period. The evaporation coefficient of stage 3 is the largest. However, at stage 2, the soil evaporation coefficient 0.78 obtained by the remote sensing PM model is smaller than the result 0.88 at stage 1, which indicates that the soil evaporation coefficient of the model during the simulation period is not a simple linear correlated with the surface soil moisture content, and the model calibration results are uncertain.

Tab. 1　Parameter calibration of different periods

Soil moisture interval	Parameter calibration resultsf	
	f	g_{sx}
Stage 1	0.883 9	0.009 7
Stage 2	0.782 9	0.043 3
Stage 3	1	0.050 0

There are many reasons for the uncertainty of parameter calibration results. The first is the optimization algorithm. In this paper, a simulated annealing algorithm is used to calibrate the sensitive parameters of remote sensing P-M. The initial population is set to 50, and the maximum number of iterations is set to 20. The selection of different parameters in the algorithm may have an impact on the results of calibrated parameters. Secondly, the accuracy of the SMAP surface soil moisture data will affect the division of stages. Finally, the selection of the sensitive parameter interval will also affect the results of parameter calibration. Based on the existing research results, the interval of f and g_{sx} is [0.050, 1.000] and [0.002, 0.050], respectively.

2.3　Relationship between changes in soil water content and evaporation

In order to further analyze the influence of different surface soil moisture content on soil evaporation, the parameters described in Section 2.1 are used to calculate the soil evaporation and vegetation emission for each stage. The main crops are winter wheat and summer corn at Wangdu station.

However, the stage division in this study is based on the soil moisture content, and the same stage may contain different seasons. Therefore, this section mainly analyzes the relationship between soil moisture content and evaporation. Fig. 6 (a) shows the comparison of soil evaporation in different stages, where the horizontal axis is the serial number generated from low to high SMAP soil moisture content at each stage (excluding non-evapotranspiration observation dates and remote sensing date when the data is an invalid value). According to the soil moisture content, different stages are divided to analyze the changes of soil evaporation and vegetation emission under different soil moisture conditions. Judging from the division of the three stages, the higher the soil moisture content, the greater the soil evaporation. This phenomenon is more obvious in stage 1. The soil moisture content in stage 1 is the lowest as a whole, and the soil evaporation is also low in the three stages. From the perspective of the daily average soil evaporation in each stage (Tab. 2), the daily average soil evaporation in stage 1 is 0.139 6 mm /d, which is also the lowest in the three stages. This is because the soil evaporation is mainly the water loss process of the soil, and 0-20 cm is the soil layer strongly affected by the soil evaporation. When the soil water supply condition is good, the soil water will be fully evaporated. As the continuous state of the capillary, the soil evaporation will gradually reduce when the soil water content is less than the field water capacity[27].

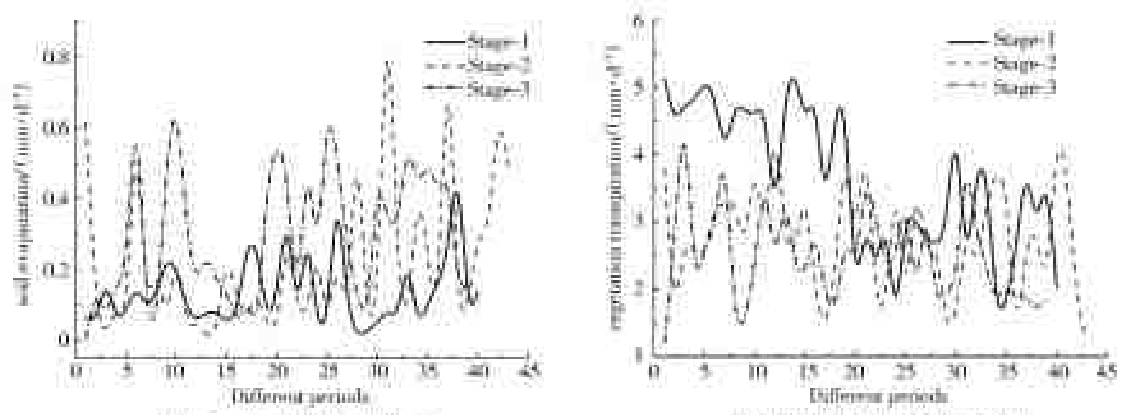

(a) Changes of soil evaporation (b) Change of vegetation emission

Fig. 6 The variation of soil evaporation and vegetation transpiration for different periods at Wangdu station from May to October in 2018

Tab. 2 The average values of soil evaporation and vegetation transpiration in different periods

Soil moisture interval	Soil moisture content range/($cm^3 \cdot cm^{-3}$)	Mean value of soil evaporation/($mm \cdot d^{-1}$)	Mean value of vegetation emission/($mm \cdot d^{-1}$)
Stage 1	(0.044 7, 0.076 8)	0.139 6	3.652 1
Stage 2	(0.076 8, 0.106 4)	0.221 9	2.754 9
Stage 3	(0.106 4, 0.212 5)	0.297 9	2.509 4

During the simulation period, the correlation between the amount of surface soil water content and changes in vegetation emission was poor. From Fig. 6 (b), it can be seen that in stage 1 with the lowest soil moisture content of SMAP, the simulation results of vegetation emission are the highest in many simulation days, especially in the first 20 simulation days of stage 1. In addition to soil water content, vegetation emission is also affected by factors such as temperature, sunlight, and plant physiological characteristics. Because this study segmented the simulation period according to the SMAP surface soil water content, the growth period is discontinuous within each segment, and meteorological conditions are not taken into account during the stage division, which resulted in insignificant changes in vegetation emission.

As mentioned above, the soil layer 0-20 cm above the ground surface is the soil layer with strong soil evaporation. However, due to the limitation of remote sensing observation depth, the SMAP microwave product which is selected in this paper cannot reflect the soil water status at 20 cm depth, only as an approximation of the soil water content at 10 cm above the ground surface. Therefore, the analysis of this study only focuses on the effect of changes in surface soil moisture on evapotranspiration, and the study of the relationship between soil moisture and evapotranspiration at a depth of 10-20 cm can be based on assimilated products of soil moisture (such as GLDAS, etc.), and related work will be carried out in subsequent studies.

2.4　Uncertainty analysis of model parameters

In order to further analyze the uncertainty of the model parameters, this study analyzes the influence of parameter selection on simulation results based on the GLUE algorithm. The f and g_{sx} parameters were measured according to the Monte Carlo method, and a total of 10,000 samples were taken. Fig. 7 shows the comparison between the values of the two sensitive parameters and the results of the likelihood function being greater than the threshold. It can be seen that the parameters f and g_{sx} both obey the exponential distribution, and the value interval of f is concentrated between 0.78 and 0.99. The larger the value of g_{sx}, the greater the probability that the model will obtain a higher likelihood value. In comparison, the parameter f has greater uncertainty on the model. The results of the three uncertainty indicators of the model show CR value is 32, the B value is 0.63 (mm/d), the S value is 1.25, respectively, and the correlation between the evapotranspiration simulation value and the uncertainty interval also shows that part of simulation value is outside the uncertainty interval (the evapotranspiration interruption part in the figure is the missing date for monitoring) (Fig. 8), so the model parameters are uncertain[28].

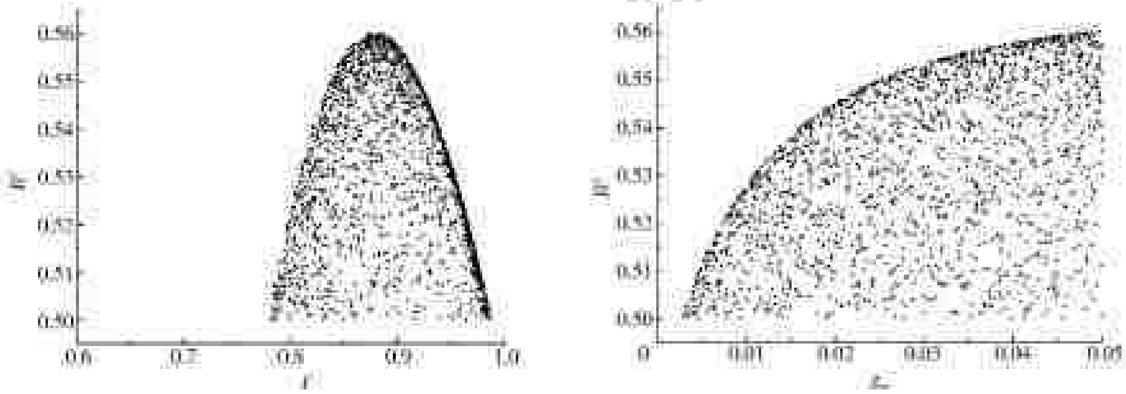

Fig. 7　Scatter plots of likelihood function values for sensitive parameters

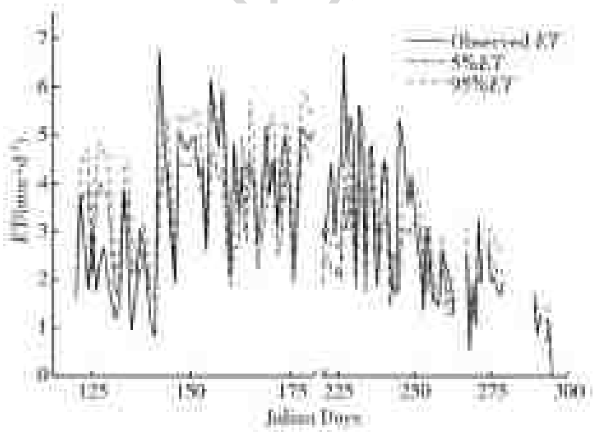

Fig. 8　Uncertainty interval of daily evapotranspiration at a 90% confidence level

In general, the remote sensing P-M model well simulates the evapotranspiration process for Wangdu station and has high simulation accuracy. However, due to factors such as the prior distribution selection rules of the model parameters, model structure, sampling rules, and input data errors, there are still some uncertainties in the simulation process, and the model does not fully simulate the evapotranspiration process.

3　Conclusions

In this paper, the remote sensing P-M model was used to invert the evapotranspiration of Wangdu station from May to October, and the effects of changes in surface soil moisture on the calibration of model parameters and soil evaporation and vegetation emission are analyzed with SMAP surface soil moisture products. The main conclusions are as follows

(1) Based on the remote sensing P-M model, the evapotranspiration of Wangdu station from May to October 2018 is simulated. The NSE coefficient of the simulated and measured values is 0. 56. This method has a good simulation ability for evapotranspiration at Wangdu station.

(2) When the remote sensing P-M model has the highest soil moisture content, the calibration result of the soil evaporation coefficient reaches the maximum value, but there is still uncertainty between the two.

(3) In the case of only considering the change of surface soil moisture content, the consistency between soil moisture content and soil evaporation is obvious, but the consistency between soil moisture content and vegetation emission is weak under the influence of meteorological conditions, vegetation growth period and other factors.

(4) The uncertainty analysis of the model parameter in calibration shows that although the simulated evapotranspiration results can better reflect the actual observation situation, the remote sensing P-M model has certain uncertainty, and the uncertainty of the sensitive parameter f is greater.

References:

[1] LI F, SHEN Y J. Progress in remote sensing-based models for surface heat and water fluxes[J]. Resources Science, 2014, 36(7): 1478-1488. (in Chinese) DOI: 1007-7588(2014)07-1478-11.

[2] XIN X Z, TIAN G L, LIU Q H. A review of researches on remote sensing of land surface evapotranspiration [J]. Journal of Remote Sensing, 2003, 7(3): 233-240. (in Chinese) DOI: 1007-4619(2003)03-0233-08.

[3] ZHANG F Y, WANG F M, ZHOU B, et al. Study on evapotranspiration estimation of Zhejiang Province based on SEBAL model[J]. Yangtze River, 2013, 44 (17): 40-44. (in Chinese) DOI: 1001-4179(2013)17-0040-05.

[4] FENG J Z, WANG Z J. A review on evapotranspiration estimation models using remotely sensed data[J]. Shuili Xubao, 2012, 43(8): 914-925. (in Chinese) DOI: 0559-9350(2012)08-0914-12.

[5] WANG Y J, SUN D F. Review of the regional evapotranspiration estimation using remote sensing[J]. Transaction of the CSAE, 2005, 21(7): 162-167. (in Chinese)) DOI: 1002-6819(2005)07-0162-06.

[6] SU Z. The surface energy balance system (SEBS) for estimation of turbulent heat fluxes[J]. Hydrology and Earth System Sciences, 2002, 6(1): 85-99. DOI: 10. 5194/hess-6-85-2002.

[7] BASTIAANSSEN W G M, MENENTI M, FEDDES R A, et al. A remote sensing surface energy balance algorithm for land (SEBAL)-1. Formulation[J]. Journal of Hydrology, 1998, 212 (1-4): 198-212. DOI: 10. 1016/S0022-1694(98)00253-4.

[8] GUO X Y, CHENG G D. Advances in the application of remote sensing to evapotranspiration research in arid regions[J]. Advances in Earth Science, 2011, 26 (8): 848-858. DOI: 10. 11867/j. issn. 1001-8166. 2011. 08. 0848.

[9] CLEUGH H A, LEUNING R, MU Q Z, et al. Regional evaporation estimates from flux tower and MODIS satellite data[J]. Remote Sensing of Environment, 2007, 106: 285-304. DOI: 10. 1016/j. rse. 2006. 07. 007.

[10] MU Q Z, HEINSCH F A, ZHAO M S, et al. Development of a global evapotranspiration algorithm based on MODIS and global meteorology data[J]. Remote Sensing of Environment, 2007, 111, 519-536. DOI: 10. 1016. /j. rse. 2007. 04. 015.

[11] WANG H B, MA M G. Estimation of transpiration and evaporation of different ecosystems in an inland river basin using remote sensing data and the Penman-Monteith equation[J]. Acta Ecologica Sinica, 2014, 34(19): 5617-5626. (in Chinese) DOI: 10. 5846/stxb201301150102.

[12] LEUNING R, ZHANG Y Q, RAJAUD A, et al. A simple surface conductance model to estimate regional evaporation using MODIS leaf area index and the Penman-Monteith equation[J]. Water Resources Research, 2008, 44, W10419. DOI: 10. 1029/2007WR006562.

[13] ZHANG Y Q, CHIEW F H S, ZHANG R, et al. Estimating catchment evaporation and runoff using MODIS leaf area index and the Penman-Monteith equation[J]. Water Resources Research, 2008, 44(10), DOI: 10. 1029/2007wr006563.

[14] LI H X, ZHANG Y Q, ZHANG X H, et al. Estimation of regional transpiration and evaporation using Penman-Monteith equation[J]. Engineering Journal of Wuhan University, 2011, 44(4): 457-461. (in Chinese) DOI: 1671-8844(2011)04-0457-05.

[15] ZHANG Y Q, CHIEW F H S, PENA-ARANCIBIA J, et al. Global variation of transpiration and soil evaporation and the role of their major climate drivers[J].

Journal of Geophysical Research: Atmospheres, 2017, 122, 6868-6881. DOI: 10.1002/2017JD027025.

[16] WANG Z H. Analysis of the changing rules of cropland evapotranspiration[J]. Hydrology, 2005, 25(3): 35-37. (in Chinese) DOI: 1000-0852(2005)03-0035-03.

[17] CHAN S K, BINDLISH R, E. O'NEILL P, et al. Assessment of the SMAP passive soil moisture product [J]. IEEE Transactions on Geoscience and Remote Sensing, 2016, 54(8): 4994-5007. DOI: 10.1109/tgrs.2016.2561938.

[18] MONTEITH J L. Evaporation and environment//The State and Movement of Water in Living Organisms. Symposium of the Society for Experimental Biology [M]. England: Cambridge University Press, 1965, 19: 205-234.

[19] LEUNING R. A critical appraisal of a combined stomatal-photosynthesis model for C3 plants[J]. Plant, Cell and Environment, 1995(18): 339-355. DOI: 10.1111/j.1365-3040.1995.tb00370.x.

[20] ALLEN R G, PEREIRA L S, RAES D, et al. Crop evapotranspiration: Guideline for computing crop requirement[M]. Irrigation and Drainage, Rome, Italy, 1998, FAO.

[21] ZHU Z Y. Evapotranspiration models and water requirements of nature vegetation in the arid and semi-arid region[D]. Huhhot: Inner Mongolia Agricultural University, 2005. (in Chinese)

[22] NASH J E, SUTCLIFFE J V. River forecasting using conceptual models, 1. A discussion of principles[J]. 1970, 97: 337-351.

[23] KELLIHER F M, LEUNING R, RAUPACH M R, et al. Maximum condunctances for evaporation from global vegetation types[J]. Agricultural and Forest Meteorology, 1995(73): 1-16.

[24] BEVEN K, BINLEY A. The future of distributed models: model calibration and uncertainty prediction [J]. Hydrological Processes, 1992(6): 279-298. DOI: 10.1002/hyp.3360060305.

[25] JIANG M Y. A predication model of BP neural network based on genetic simulated annealing algorithms [J]. Software Engineering, 2018, 21(7): 36-38. (in Chinese) DOI: 2096-1472(2018)-07-36-03.

[26] JIA Y C, XIE M W, JIANG H T. Daily estimation of global 36 km grid soil moisture[J]. Journal of Geo-information Science, 2017, 19(6): 854-860. (in Chinese) DOI: 10.3724/SP.J.1047.2017.00854.

[27] RUI X F. Principles of Hydrology[M]. Beijing: China Water Power Press, 2004. (in Chinese)

[28] WANG H J, XIAO W H, WANG Y C, et al. Assessment of the impact of climate change on hydropower potential in the Nanliujiang River basin of China[J]. Energy, 2019(167): 950-959. DOI: 10.1016/j.energy.2018.10.159.

(上接第 30 页)

[32] XU J. Variation in annual runoff of the Wudinghe River as influenced by climate change and human activity[J]. Quaternary International, 2011, 244(2): 230-237. DOI: 10.1016/j.quaint.2010.09.014.

[33] WANG L X, ZHANG Z Q. Impacts of forest vegetation on watershed runoff in dryland areas[J]. Journal of Natural Resources, 2001, 16(5): 439-444. (in Chinese) DOI: CNKI: SUN: ZRZX.0.2001-05-007.

[34] YANG Y, SHANG S, JIANG L. Remote sensing temporal and spatial patterns of evapotranspiration and the responses to water management in a large irrigation district of north China[J]. Agricultural and Forest Meteorology, 2012, 164: 112-122. DOI: 10.1016/j.agrformet.2012.05.011.

[35] ZHANG S L, YANG D W, YANG H B, et al. Analysis of the dominant causes for runoff reduction in five major basins over China during 1960-2010[J]. Advances in Water Science, 2015, 26(5): 605-613. (in Chinese) DOI: 10.14042/j.cnki.32.1309.2015.05.001.

[36] WANG B W. Research on the runoff response to underlying surface changes in upper Luanhe River basin [D]. Tianjin: Tianjin University, 2018. (in Chinese)